Low Cost Adaptive Optics Testbed for Small Telescopes

Manuel Cegarra and Andrew Lambert
School of Engineering and IT, UNSW Canberra, Northcott Drive, Canberra ACT 2600, Australia

Keywords: Atmosphere Turbulence, Deformable Mirror, FPGA, Wavefront Sensor.

Abstract: The aim of this work is the development of a low cost Adaptive Optics system that can be used as a testbed for laboratory research installed on a small telescope. An optical system has been designed supported in a mechanical structure, and a control system has been developed and installed in a FPGA reconfigurable platform. Particular premises specific to small telescopes have been considered in the design and development stages, such as the use of low cost optical and electronic components, and the portability and lightness of the platform. Laboratory tests successfully validate that the whole control system can be implemented in a low cost standalone FPGA device and that an optical subsystem mounted in a configurable and lightweight structure can be used for laboratory test and telescope use.

1 INTRODUCTION

Adaptive Optics (AO) can be considered a technique to compensate the aberrations in the wavefront of a light beam that travels through a medium. One of its main applications is astronomy, although it could be also applied in, for instance, surveillance, ophthalmology or microscopy. In the case of astronomy, these aberrations are produced by the atmospheric turbulence, due to terrestrial surface heating.

AO doesn't have a long history. Its origins date back around the 1950's. Firstly it was promoted by astronomical associations and defence governmental departments, and in the last 30 years has suffered a rapid evolution, in part due to the enhancements experimented by computer processing, sensors and actuators, which are the three main technologies on which adaptive optics is based (Tyson, 2000). In the mid-90s AO systems were only in the planning stages for the current big telescopes (with diameter bigger than 3 metres).

Nowadays the high budget astronomy is strongly dependant on AO systems. This sector of astronomy comprises big telescopes in observatories spread all over the world. Also, bigger telescopes (Extremely Large Telescopes, ELT) from 20 to 100 metres in diameter, are currently under construction. These ones will require complex AO systems.

Less research has been performed in the medium and low budget astronomy sector, which can be considered formed by small research installations, medium size observatories, universities and amateur astronomy. In general terms, AO is expensive. It consists of precise and well designed opto-mechanical components, where alignment and precision are fundamental issues, and the more expensive the components, the better performance the system will have, requiring a reasonable budget, research work and engineering work in several fields, as electronics, optics, or mechanics.

The hypothetical performance of an AO system in a small telescope has to be considered. In this kind of telescope, less photons are introduced in the system and resolution is lower, which could raise some doubts about the advantages of the use of AO systems in this sector.

However, currently some commercial AO systems for small telescopes are available such as the commercialized by Santa Barbara (http://www.sbig.com/Adaptive-Optics/) and Stellar Products (http://www.stellarproducts.com/). These systems are intended to correct low order local atmospheric effects. Other companies have developed more versatile solutions (http://www.okotech.com/ao-systems, http://www.bostonmicromachines.com/aosolutions.htm).

The concept of a low cost AO system for its use in medium and small size telescope has been developed by different authors, proposing various optic and computer control configurations

Cegarra M. and Lambert A..
Low Cost Adaptive Optics Testbed for Small Telescopes.
DOI: 10.5220/0004337900450051
In *Proceedings of the International Conference on Photonics, Optics and Laser Technology* (PHOTOPTICS-2013), pages 45-51
ISBN: 978-989-8565-44-0

(Aceituno, 2009); (Loktev et al., 2008); (Teare et al., 2006).

Although the control of first AO systems were designed using traditional CPU (Central Processing Unit) architectures, advances in computer processing, with the emergence of other kind of electronic devices as Field Programmable Gate Array (FPGA) or Graphics Processing Unit (GPU) changed dramatically the approach to this issue. FPGA technology was considered some years ago as an option to implement the control algorithm, due to its inherent pipeline and parallel design possibilities, low cost, and high speed architectures. FPGA devices can be easily reprogrammed, providing a high degree of flexibility in the development phase. The reduced size of devices nowadays has decreased the overall size of electronic architectures, opening possibilities to more lightweight AO systems, which could be used in small telescopes.

During the last 10 years several research teams have worked in the proposal of electronic architectures which use FPGA as central processing unit (Peng et al., 2008); (Rodriguez-Ramos et al., 2006); (Saunter et al., 2005). In AO control several stages are involved, being some of them of high computational requirements, as VMM (Vectorial Matrix Multiplication), in order to obtain the reconstructed wavefront. Reconstruction algorithms require an iterative process, thus making them appropriate for pipeline and parallel processing, so they are suitable for implementation in Digital Signal Processor (DSP), GPU and FPGA devices.

Research efforts in control systems have mainly targeted high-end FPGA devices, because their use was intended for AO systems installed in big telescopes, where the cost of the electronic architecture was a minor problem in the overall cost of the project. Nevertheless, some authors have focused in low cost FPGA devices and have proved that latency times can also be reduced, even with these kind of devices, and have opened the possibility to their use as a standalone device within an AO system (Kepa et al., 2008).

2 AO FUNDAMENTALS

2.1 Atmosphere Turbulence

Atmosphere turbulence is the main parameter to limit the resolution of Earth based telescopes. Air masses of different sizes moving at various speeds produce variations in the refraction index of the incoming wavefronts. As a consequence, these variations modify the intensity and phase of the wavefront, resulting in scintillation and blurry images. One way to measure the turbulence extension is through the ratio D/r_0, where D is the diameter of the telescope and r_0 is the Fried coherence length, which is a parameter describing the spatial extent of the turbulence. In high mountains, where air is less turbulent, this ratio scales with telescope diameter. Nevertheless, in poorer air, small telescopes have similar D/r_0 as large ones.

Current AO systems reach boundaries in the isoplanatic area, which is the region of the observation field where relative changes in the atmospheric turbulence can be deprecated. Due to this limitation, in recent years some researchers have focused in the way to correct aberrations beyond the isoplanatic area, that is, in wide field of view, and solutions as MCAO (Multiple Conjugate Adaptive Optics) and MOAO (Multiple Object Adaptive Optics) have arisen.

MOAO, MCAO, or hybrid solutions increase the number of optical elements in the AO systems, turning it into a more complicated system to design, to control or to manage. While this is of some importance in a big telescope, in a low cost small system this is a big issue, so a study and assessment of other options in these systems needs to be addressed. Some authors have proposed the use of a software approach to extent the isoplanatic patch, as RNN (Recurrent Neural Network), removing the need of an optical solution (Weddell, 2010).

2.2 AO System

A traditional AO system is composed of three main components: control system, wavefront sensor (WFS) to measure the aberrations, and deformable and tip-tilt mirrors to correct them mechanically. The control system, which is implemented in CPU or other dedicated hardware resource, obtains gain and phase information of the incoming wavefront from the sensor, and processes it in order to obtain signals that will be applied to the actuators of the deformable and tip-tilt mirrors, to reproduce a conjugate to the aberrated wavefront. This is a real time closed loop process.

In order to achieve the real time requirement of the feedback loop, the whole computation time has to be within the variation rate of the refraction index distortions introduced by atmosphere, typically 10 ms for well sited telescopes, but potentially much shorter for the situations considered herein.

There is a balance to ensure maximum possible light gets to the science camera. There are several kinds of wavefront sensors based in different techniques, as Shack-Hartmann, pyramidal or curvature. One of the more widespread, due to its ease of implementation is the Shack-Hartmann. In this sensor the beam goes through a lenslet array, which divides it into several small beams corresponding with each of the subapertures. The detector (usually a CMOS (Complementary Metal Oxide Semiconductor) or CCD (Charged Coupled Device) image sensor) is positioned in the focal plane of these beams. The positions of the focused beams deviate when an aberrated beam is introduced in the system, with respect the positions obtained with a non-aberrated beam. A measurement of the local slopes of the beam phase for each subaperture can be obtained from these deviations, as shown in figure 1, where gray dots and black dots represents centroids from a non-aberrated and an aberrated wavefront respectively.

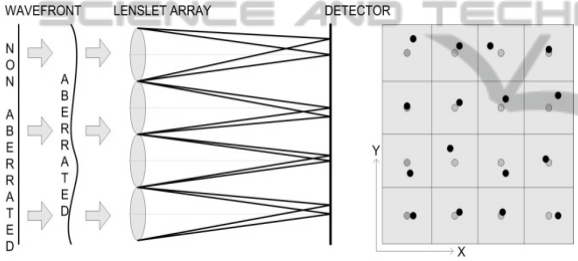

Figure 1: (Left) Shack-Hartmann wavefront sensor. (Right) Movement of sensor image within lenslet array.

Calculation of the deviation could be performed by several algorithms. CoG (Center of Gravity) calculation is a straightforward method to obtain these deviations (Fusco et al., 2006). Although it has some limitations with real spots, it is well suited for the purpose of this work.

If W(x,y) is the wavefront captured in the detector with respect to axis x and y, by geometry these differences can be related with the corresponding slopes in each of the subapertures.

$$\frac{\partial W(x,y)}{\partial x} = \frac{\Delta x(x,y)}{\mathrm{f}} \tag{1}$$

In equation 1 this relation is expressed in x axis, where Δx(x,y) is the gradient in the centroid position in x axis for a subaperture, and f is the focal distance of each of the lens of the lenslet array. A similar equation exists for y gradients.

2.3 Reconstruction Process

The control system receives the positions of the focused beams of each subaperture from the detector, and its aim is to produce the signals that will be sent to the actuators of the tip-tilt and deformable mirrors, with minimum latency.

To reconstruct the aberrated wavefront, a modal approach can be used, whereby W(x,y) can be expressed as a weighted sum of Zernike polynomials, with each of terms representing a different optical aberration, as follows:

$$W(x,y) = \sum_{i=0}^{N} w_i Z_i(x.y) \tag{2}$$

In equation 2, term w_i represents the Zernike coefficients of each of the aberrations, $Z_i(x,y)$ the Zernike polynomials, and N the number of aberrations polynomials considered.

From equations (1) and (2), the gradients of each of the subapertures can be related with a weighted sum of Zernike polynomials, as follows:

$$\frac{\Delta x(x,y)}{\mathrm{f}} = \sum_{i=0}^{N} w_i \frac{\partial Z_i(x,y)}{\partial x} \tag{3}$$

Considering all the subapertures in both axes, equation (3) can be expressed in matrix form as follows:

$$\boldsymbol{\Delta}_{2\mathrm{k\,x\,1}} = \boldsymbol{Z}_{2\mathrm{k\,x\,N}} \boldsymbol{W}_{\mathrm{N\,x\,1}} \tag{4}$$

If k is the number of subapertures, in equation (4) Δ is the gradients matrix with 2k × 1 dimensions, **Z** is the partial derivative of Zernike polynomial matrix in both axes of dimensions 2k × N, and **W** is the Zernike coefficients matrix of dimensions N × 1.

In order to obtain the Zernike coefficients from equation (4), least square estimation method could be applied to obtain the pseudoinverse matrix of **Z**, resulting in equation (5).

$$\boldsymbol{W}_{\mathrm{N\,x\,1}} = \boldsymbol{C}_{\mathrm{N\,x\,2k}} \boldsymbol{\Delta}_{2\mathrm{k\,x\,1}} ; \boldsymbol{C} = (\boldsymbol{Z}^T \boldsymbol{Z})^{-1} \boldsymbol{Z}^T \tag{5}$$

In equation (5) **C** is called the calibration matrix, with dimensions N × 2k.

In order to obtain the signals to be applied to the mirrors actuators, the influence functions have to be derived, each of them representing the bidimensional profile generated for each of the actuators. Each of the actuators will have a value to represent each of the Zernike coefficients. The matrix which relates these parameters is called influence matrix, **I**.

Finally, from equation (5) and the influence matrix, the voltages required by the actuators to reproduce a specific wavefront can be obtained as

follows:

$$\boldsymbol{V}_{1\,x\,j} = \boldsymbol{W}^{T}_{1\,x\,N}\mathbf{I}_{N\,x\,j} \quad (6)$$

In equation (6) **V** is the voltages actuator matrix, and j is the number of actuators.

3 AO PLATFORM

In order to assess the feasibility of a low cost AO system to be implemented, a mechanical support has been developed, with an attached optical setup. Below is a detailed description of each subsystem, mechanical support, optical setup and control system.

3.1 Mechanical Support

The first stage is the definition of the mechanical constraints that affect the system. The structure had to be lightweight, thus having the lowest impact as possible in the overall telescope weight together with the AO system, in order to ease the balance of the system. At the same time, the support at the junction of optical structure with telescope rear port had to be solid enough to support a weight which will be around 10 kg, which is the expected average weight of the AO system, including optical components, electronic board and the structure itself. The main aspect which needs to be addressed is that it must have enough flexibility to accommodate different optical components at different distances between them for experimentation. Also the size of the AO structure has to be small enough to be considered portable.

The weight of the platform without optics and electronic components is 4.5 kg, and the total estimated weight is 10 kg. The dimensions of the platform are 470 × 350 × 100 mm. Figure 2 shows the 3D model of the AO system prototype.

3.2 Optical Setup

The optics subsystem is modelled to evaluate the performance of the whole system in closed loop under test conditions.

The laboratory test and validation conditions evaluate the system with a laser light source, optically aligned with the optical setup, so there is no need to consider at this stage the tip-tilt correction of the beam. Not considered yet are the weak photon flux and the light incoherence of the light coming from an astronomical source. The laser light source generates a high intensity and

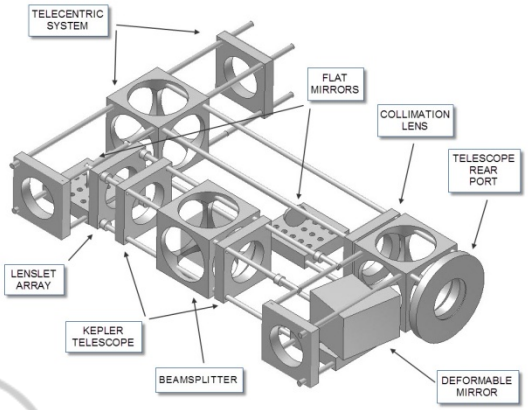

Figure 2: Mechanical testbed 3D model.

correctly aligned beam, to evaluate the capacity of the optical system and generate a valid centroids pattern, which will be used by the control system to generate the appropriate signals for the deformable mirror actuators.

Figure 3 shows the optical setup of the AO system. All lenses of the optical setup are plano-convex with 1" or 2" diameter, anti-reflection coated for 350 to 700 nm and the substrate material is N-BK7 (grade A). Flat mirrors have more than 90% average reflectivity and flatness below $5\lambda/in^2$. Here is a description of the components and main points of the optical setup.

P1: Telescope emulation. A f/10 telescope has been emulated with a HeNe Class 2 laser source, with 0.5 mW output power, forming an image at F1.

Fi1: A neutral density filter is used to decrease the laser intensity which could saturate the image in the detector.

L1: Collimation lens with focal length 200 mm. This lens collimates the beam to a diameter appropriate to illuminate the deformable mirror effective surface.

M1: A flat mirror which directs the beam to the deformable mirror. In the next stage of the project this mirror will be substituted by a tip-tilt mirror system, to correct the first order aberrations of the incoming beam.

M2: An OKO 30 mm 19-channel piezoelectric deformable mirror. The beam encompasses the effective surface of the mirror.

L2, L3: A Kepler telescope. Focal lengths of L2 and L3 are 100 mm and 50 mm respectively. This telescope system selects the beam diameter which will illuminate the lenslet array, resulting in different number of centroids in the wavefront sensor. In order to get this feature, L3 could be exchanged with

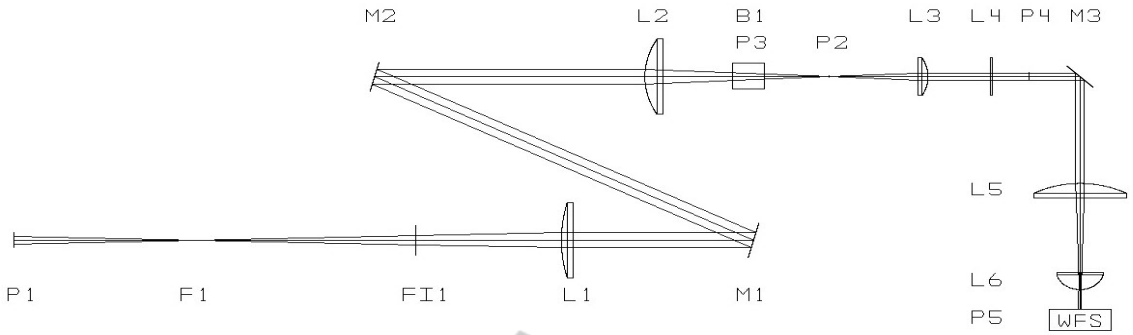

Figure 3: Optical setup. P1: position of the telescope. F1: focal plane of telescope. FI1: neutral density filter. L1: collimation lens. M1, M3: flat mirrors. M2: deformable mirror. L2, L3: Kepler telescope. B1: beamsplitter. P2, P3: Focal plane of corrected image. L4: lenslet array. P4: focal plane lenslet array. L5, L6: telecentric system. P5: WFS focal plane. WFS: wavefront sensor.

lenses with different focal lengths.

B1: Beamsplitter to divide the incoming beam in two parts, one used to generate the centroids, and the other to register or visualize the corrected image in the science camera (nitrocellulose pellicle beamsplitter of 2" 45%R 55%T).

P2, P3: Focal plane of the corrected telescope emulator image. P3 is the science camera, needed to register the corrected images.

L4: Lenslet array. It consists on a plano-convex set of 0.5 x 0.5 mm square array of lenses, and focal distance 23 mm.

P4: Focal plane of the elements of the lenslet array.

M3: Another flat mirror to adapt the optical design to the mechanical constraints of the platform.

L5, L6: These two lenses comprise a telecentric optical system. Focal lengths of L5 and L6 are 100 mm and 25.4 mm respectively. This system is used to adapt the size of the incoming beams from the lenslet array at the appropriate scale of the wavefront sensor detector.

P5: Reimaged focal plane on the wavefront sensor detector, which consists in a Pixelinx PL-A741 monochrome camera with 1.3 megapixel resolution (1280 × 1024), and 6.7 x 6.7 μm pixel size.

Figure 4 shows the geometric image analysis in the focal plane of the centroids, at 0 and 0.65 degrees input angle. Note the lateral shift in the centroids positions with input angle, while figure 5 shows the image from the wavefront sensor camera obtained in the lab from which the centroids can be determined. The centroids shapes exhibit similar distortion off-axis, compared to predicted in simulation results shown in figure 4.

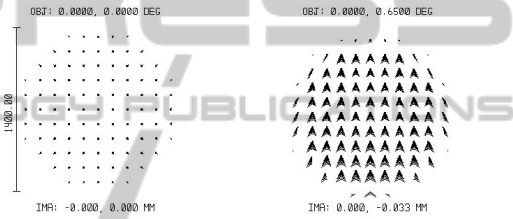

Figure 4: Spot diagram at 0 (left) and 0.65 (right) degrees input angle.

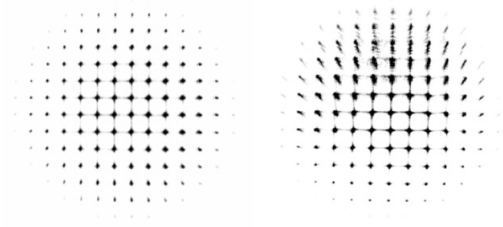

Figure 5: Image captured by WFS camera containing spots to be centroided on axis (left) and off axis (right).

3.3 Control System

In this section the control algorithm is discussed, and simulation results comparing floating point and fixed point precision are shown. Also experimental results from implementation in the FPGA device are presented.

3.3.1 Control Algorithm Architecture

The electronic top level architecture and the main blocks with comprise the FPGA control board are shown in figure 6.

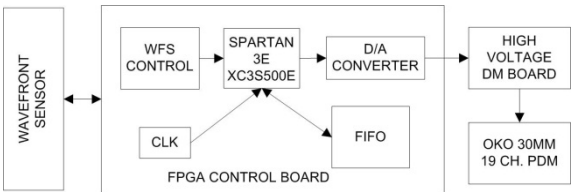

Figure 6: Top level electronic architecture, showing the relationships between the main blocks of the system.

The wavefront sensor is programmed into the FPGA control board, in order to generate the appropriate clock and data signals. The signals will be obtained through the control algorithm, to send to the high voltage deformable mirror drive board for the voltages required by the deformable mirror.

The FPGA processes the signals provided from the wavefront sensor block, and the signals to the deformable mirror actuators will be serialized and sent to the D/A converters on the drive board.

The control algorithm of the electronic architecture has been programmed in VHDL (VHSIC Hardware Description Language) and implemented in a FPGA Spartan3E XC3S500E.

Figure 7 is an illustration of the block diagram of the control algorithm implemented in the FPGA. Mathematical operations are represented as light gray blocks, while clear blocks represent preloaded data in FPGA embedded or distributed RAM (Random Access Memory). The DATA FLOW CONTROL block (in dark gray) manages the data flow along the process, generating control logic, delays and the appropriated enable and reset signals to each segment of the process.

3.3.2 Floating Point vs. Fixed Point

The FPGA shares resources in a time division multiplexing process, taking advantage of the per clock basis nature of the process, using pipeline when is required. Parallel processing is performed in the X and Y axis computation blocks where appropriate, with the aim to get the minimum latency time at the end of each frame processing.

In order to get high computation speed, FPGA operations are performed with a fixed point resolution. To assess the accuracy of the obtained data, two models were designed in MATLAB, one with double floating point resolution, and the other with fixed point. In the whole computation process, the selection of the number of bits for the fractional part of the divisions is a key parameter which affects both resolution and utilization of hardware FPGA resources.

A synthetic image was created, in order to generate centroids in random positions, which affects all the Zernike modes considered. A 300 x 300 pixel image was created, subdivided in 10 x 10 subapertures, hence each of the subapertures consist of 30 x 30 pixels squares. Nine Zernike modes were considered, but not piston movement, resulting in Zernike coefficients from W1 to W9.

Figure 8 shows the relative error in tip and tilt modes of Zernike coefficients (W1 and W2), when fixed point resolution with different number of bits in the fractional part is selected, compared to floating point precision. These differences have been evaluated for three tip-tilt slope severity levels, corresponding to 1 pixel, 7 pixels and 14 pixels displacement of the centroids.

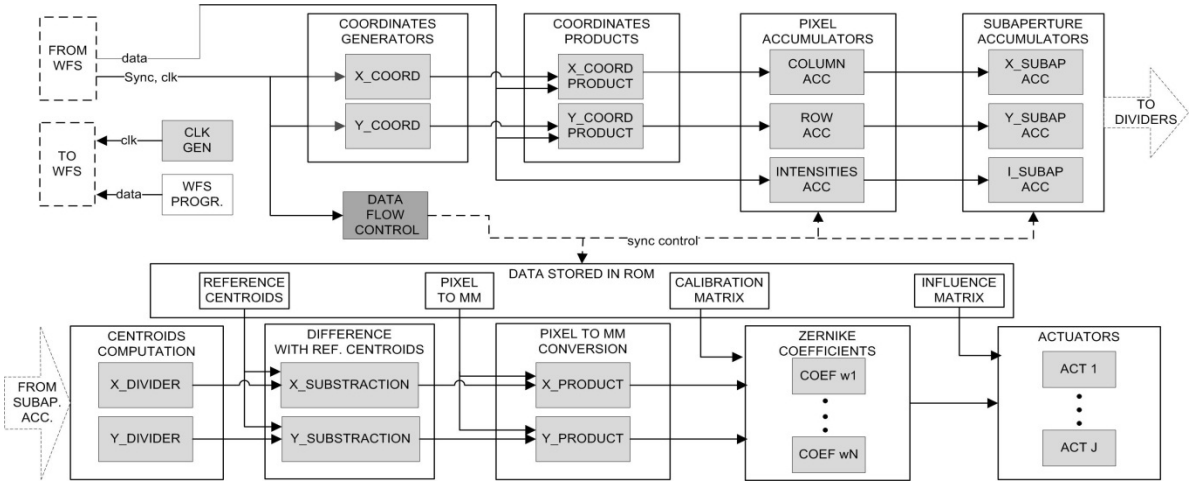

Figure 7: Blocks diagram of FPGA control algorithm.

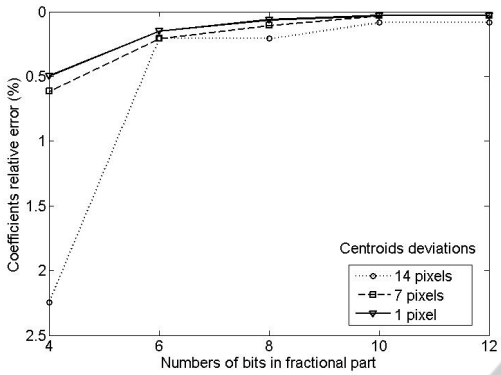

Figure 8: Error in W1 and W2 Zernike coefficients with different number of bits in the fractional part, compared with floating point precision.

Notice that error introduced by the use of fixed point resolution with 10 bits or more in the fractional part is independent of the number of extra bits. Below 6 bits, the relative error increases more dramatically. This analysis does not include PSF (Point Spread Function) distortion.

The fixed point model with 10 bits in the fractional part was synthesized in a Spartan 3E XC3S500E and in table 1 is shown the FPGA utilization summary, indicating that the control system can be implemented in a low capacity FPGA. Auxiliary tasks can be included.

Table 1: FPGA utilization summary, showing the percentage of used resources in device.

Logic utilization	Used	Available	%
Number of slice FlipFlop	6.231	9.312	67
Number of 4 input LUTs	3.693	9.312	40
Number of occupied slices	3.654	4.656	78
Number of RAMB16s	6	20	30
Number of BUFGMUXs	1	24	4
Number of MULT18x18SIOs	9	20	45

4 CONCLUSIONS

An AO platform has been developed for use with small telescopes, and tested in the laboratory. The optical configuration shows that with low cost components a flexible light path could be built. The whole control algorithm was implemented in a low cost standalone FPGA, a Spartan3E XC3S500E, without requiring extra computing devices. If more computing operations, such as filters, were required, the VHDL based code could be easily exported to a more powerful FPGA device. Results from simulation and implementation of the control algorithm shows a correct behaviour with only 60 clock cycles latency from the last pixel of a frame sent to the control system.

We are yet to examine the dynamic performance of the AO control system, taking into account delays in the mirror actuators and other parts of the system, including a tip-tilt mirror control in the FPGA.

REFERENCES

Aceituno, J. (2009). PhD Thesis, *Prototipo de sistema de óptica adaptativa basado en un espejo deformable de membrana para aplicación astronómica.* Universidad de Granada, Granada.

Fusco, T., Thomas, S., Nicolle, M., Tokovinin, A., Michau, V., & Rousset, G. (2006). *SPIE 6272, Advances in Adaptive Optics II, 627219*.

http://www.sbig.com/Adaptive-Optics/. 14-10-2012.

http://www.stellarproducts.com/. 14-10-2012.

http://www.okotech.com/ao-systems. 14-10-2012.

http://www.bostonmicromachines.com/aosolutions.htm. 14-10-2012.

Kepa, K., Coburn, D., Dainty, J., & Morgan, F. (2008). *Measurement Science Review, 8*(4), 87-93.

Loktev, M., Vdovin, G., & Soloviev, O. (2008). Paper presented at the Proc. SPIE 7015, Adaptive Optics Systems, 70153K, Marseille, France.

Peng, X., Li, M., & Rao, C. (2008). Paper presented at the Proc. SPIE 7130, 71303Z.

Rodriguez-Ramos, L. F., Viera, T., Herrera, G., Gigante, J. V., Gago, F., & Alonso, A. (2006). Art. no. 62723X. *Advances in Adaptive Optics II, Prs 1-3, 6272*, U1326-U1335.

Saunter, C. D., Love, G. D., Johns, M., & Holmes, J. (2005). *Proc. SPIE 6018, 60181G*.

Teare, S. W., Martinez, T., Andrews, J.R. (2006). Art. no. 630609. *Advanced Wavefront Control: Methods, Devices, and Applications IV, 6306*, 30609-30609.

Tyson, R. K. (2000). *Introduction to adaptive optics / Robert K. Tyson*. Bellingham, WA: SPIE Press.

Weddell, S. J. (2010). *A Thesis Presented for the Degree of Doctor of Philosophy, New Zealand*: University of Canterbury.